

Fractality in Persistence Decay: Dependence upon initial correlation in ferromagnetic ordering

Saikat Chakraborty and Subir K. Das*

Theoretical Sciences Unit, Jawaharlal Nehru Centre for Advanced Scientific Research, Jakkur P.O, Bangalore 560064, India

(Dated: February 17, 2019)

Dynamics of ordering in Ising model, following quench to zero temperature, have been studied via Glauber spin-flip Monte Carlo simulations in space dimensions $d = 2$ and 3 . Primary objective has been to understand the time decay in number of persistent spins and corresponding fractal dimensionality for varying correlations in the initial configurations prepared at different temperatures, at and above the critical value. It is observed that the fractal dimensionality and the exponent describing the power-law decay of persistence probability are strongly dependent upon the relative values of average nonequilibrium domain size and the initial equilibrium correlation length. Via appropriate scaling analyses, these quantities have been estimated for quenches from infinite and critical temperatures. The above mentioned dependence is observed to be less pronounced in higher dimension. In addition to these results for the local persistence, we present results for the global persistence as well. Scaling analyses using the latter results, in addition to providing new persistence exponents, have been useful in gaining important insights on the growth of patterns.

I INTRODUCTION

Kinetics of phase transitions [1–4] remains an active area of research for several decades. There typically one is interested in the nonequilibrium dynamics related to the evolution of a system to a new equilibrium state, having been quenched from a configuration prepared outside the coexistence curve to inside it, via the variation of temperature (T), pressure, etc. In this work, our focus is on the paramagnetic to ferromagnetic transition [5]. When a system is quenched, via variation of T , from the paramagnetic phase to ferromagnetic one, domains rich in like spins form and grow with time [2]. Aspects that drew attention of researchers, in this problem, are understanding of domain patterns [2], growth of domains [2], aging properties of the evolution [6–8], as well as the pattern (and corresponding dynamics) exhibited by atomic magnets that did not change orientation till time t , referred to as persistent spins [4, 9–24]. This work primarily deals with the latter aspect.

During the process of ferromagnetic ordering (where the order parameter is a nonconserved quantity), the average domain size, ℓ , increases as [2]

$$\ell \sim t^\alpha, \quad (1)$$

where α , the growth exponent, depends upon system dimensionality (d) and order-parameter symmetry. This growth occurs via curvature driven motion of domain boundaries, facilitated by change in orientation of the spins, S_i , the subscript i being an index related to an atom or spin, typically considered to be located on a regular lattice. In this work we study the spin-1/2 Ising model, to be defined later. In this case S_i is a scalar quantity which gets affected only via (complete) flipping or change in sign. The persistence probability, P , defined as the fraction of unaffected

spins, typically decays as [4]

$$P \sim t^{-\theta}, \quad (2)$$

where, like α , θ also has dependence upon d and symmetry of the order parameter. The persistent spins exhibit interesting fractal pattern with dimensionality [17] d_f whose dependence upon θ will be introduced later.

Unless mentioned otherwise, all our results correspond to local persistence, probability for which, as already mentioned, is calculated by counting unaffected “microscopic” spins. There has also been interest in the calculation of such probability by dividing the system into blocks of linear dimension ℓ_b and counting the persistence of coarse-grained or block spin variables [14, 15]. In the limit $\ell_b \rightarrow a$, the microscopic lattice constant, such block persistence probability, P_b , will correspond to P , the “local or site persistence” probability. On the other hand, for $\ell_b \rightarrow \infty$, one obtains “global persistence” probability, further discussion and results for which will be presented later.

For Ising model, values [2, 17, 19] of α , θ and d_f are accurately estimated, particularly in $d = 2$, for quenches from initial temperature $T_i = \infty$ to the final value $T_f = 0$. Recent focus, for persistence as well as for other aspects of coarsening, has been on [23–27] quenches from temperatures providing large equilibrium correlation length ξ . In this context, in a recent work [24], we have explored the initial correlation dependence of α and θ . Our observation was, while α is insensitive to the variation of T_i (at least in $d = 2$), P (and thus θ) is strongly influenced by the choice of the latter. While values [2, 14] of α are $1/2$ and close to $1/3$ (see discussion on this later), in $d = 2$ and 3 , respectively, irrespective of the choice of T_i , for θ we have [4, 11–19, 24] $\simeq 0.225$ and $\simeq 0.18$, in the above order of dimensions, for $T_i = \infty$, whereas

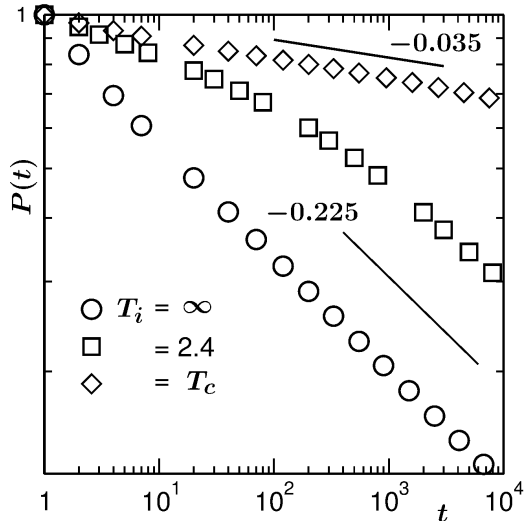


FIG. 1. Log-log plots of local persistence probability, $P(t)$, vs t , for quenches (of the Glauber Ising model) from different values of initial temperature T_i ($\geq T_c$, the critical temperature), to the final value $T_f = 0$. All results correspond to space dimension $d = 2$ and square lattice, with linear dimension of the square box being $L = 2048$, in units of the lattice constant a . The lines represent various power-law decays, values of the exponents being mentioned in appropriate places.

$\theta = \theta_c \simeq 0.035$ and $\simeq 0.105$ for $T_i = T_c$, the critical temperature (See Fig. 1 for $d = 2$). For intermediate temperatures, as seen in Fig. 1, a slower decay (with exponent θ_I that approaches θ_c as $\xi \rightarrow \infty$, i.e., $T_i \rightarrow T_c$) was observed for $\ell < \xi$. For $\ell \gg \xi$, behavior consistent with $T_i = \infty$ was obtained. The overall time decay of P , for all T_i , was empirically constructed to be [24]

$$P(t)x^{2\theta} = A \left(\frac{x}{g(x) + x} \right)^\phi; \quad x = \ell/\xi, \quad (3)$$

with

$$g(x) = \frac{C_0}{1 + C_1 x^\psi}, \quad (4)$$

where A is the amplitude of the long time decay, $\phi = (\theta - \theta_I)/\alpha$, $\psi \simeq 2$, whereas C_0 and C_1 are dimension dependent constants.

An extension of a study [17] (via a different model in $d = 1$) predicts

$$d_f = d - z\theta, \quad (5)$$

where z is a dynamical exponent related to the growth of the persistence pattern. From previous studies [24, 27], it has been reported that the decay of P is disconnected with the growth of ℓ . Nevertheless, it is unclear whether and how z , which is related to the persistence pattern, can be associated with α . Also the values of α in $d = 3$, mentioned above is not

unambiguous. In that case, even though we already have understanding about T_i dependence of θ , to gain knowledge about variation of d_f , as a function of T_i , estimation of z is needed. In this work, our objective thus, is to estimate d_f , z and α , for $T_i = \infty$ and $T_i = T_c$, in various space dimensions, for quenches to $T_f = 0$.

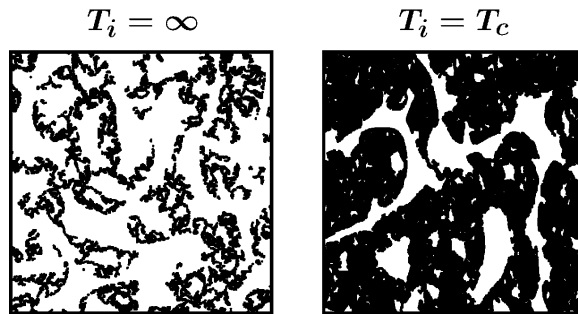


FIG. 2. Snapshots of the persistent spins are shown for quenches from $T_i = \infty$ and T_c , to $T_f = 0$. The results correspond to $d = 2$, $L = 2048$ and $t = 10^4$ MCS. In both the cases only parts of the boxes where the persistent spins are marked in black.

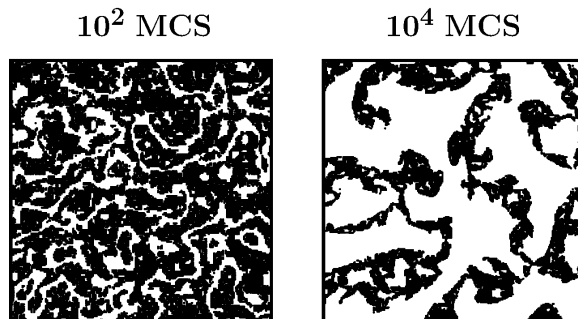


FIG. 3. Snapshots of the persistent spins from different times, mentioned on the figure, are shown for $T_i = 2.4$ and $T_f = 0$. Other details are same as Fig. 2.

In Fig. 2 we show persistence snapshots for $T_i = \infty$ and T_c , both from $t = 10^4$ Monte Carlo steps (MCS), this time unit to be defined soon, for $d = 2$ Ising model. It is clear that the patterns are different and so, different values of d_f are expected. In Fig. 3, snapshots from an intermediate temperature $T_i = 2.4$ ($> T_c$), for $d = 2$, are presented. The first frame corresponds to a time falling in the slower decay regime of Fig. 1 (for the corresponding temperature), whereas the second one is from the faster decay regime, implying $\ell \gg \xi$. The earlier time snapshot resembles the $T_i = T_c$ picture of Fig. 2 and the second one has similarity with $T_i = \infty$ pattern. This justifies our focus only on these two limiting initial temperatures with $\xi = 0$ and ∞ , rather than exploring a wide temperature range, to accurately quantify d_f and z .

The rest of the paper is organized as follows. In the

next section we describe the model and method. Section III provides a brief overview of an earlier work. Results are presented in section IV. Finally, section V concludes the paper with a brief summary and outlook.

II MODEL AND METHOD

As already mentioned, we study the Ising model [5], on square or simple cubic lattice systems, depending upon the dimensionality, with nearest neighbor interactions. The Hamiltonian for the model is given by

$$H = -J \sum_{\langle ij \rangle} S_i S_j; \quad S_i = \pm 1, \quad (6)$$

where J is the interaction strength (> 0) and $\langle ij \rangle$ implies interaction among nearest neighbors. The values of T_c for this model in $d = 2$ and 3 are respectively [28] $\simeq 2.27J/k_B$ and $\simeq 4.51J/k_B$, k_B being the Boltzmann constant.

Kinetics in this model was introduced via Glauber spin-flip mechanism [28, 29]. In this Monte Carlo (MC) approach, a trial move consists of changing the sign of a randomly chosen spin. Since our quenches were done to $T_f = 0$, a move was accepted only if it had reduced the energy. Needless to say, initial configurations were prepared at nonzero T values. In that case, the Metropolis criterion for the acceptance of a move was implemented via appropriate calculation of the Boltzmann factor [28] and its comparison with a random number, ranging between 0 and 1, whenever the move brought an increment in the energy. For initial temperatures very close to T_c , in addition to the Glauber mechanism, we have applied Wolff algorithm [30] as well, for faster equilibration. Time, in our simulations are measured in units of MCS, each MCS consisting of L^d steps, L being the linear dimension of a square or cubic box. Periodic boundary conditions were applied in all directions. Final results are presented after averaging over multiple initial realizations, the number ranging from 20 to 70.

III AN OVERVIEW OF THE BACKGROUND

In this section we provide a discussion on the theoretical background, following the work by Manoj and Ray [17].

From a density correlation function, $D(r, t)$, isotropic in an unbiased system, total mass or number of particles in a circular or spherical (depending upon dimensionality) region of radius R can be obtained as

$$M(R, t) \sim \int_0^R D(r, t) r^{d-1} dr, \quad (7)$$

r ($= |\vec{r}|$) being the scalar distance of a point in that region from the central one. An appropriate correlation function in the present context is

$$D(r, t) = \frac{\langle \rho(\vec{r}_0, t) \rho(\vec{r}_0 + \vec{r}, t) \rangle}{\langle \rho(\vec{r}_0, t) \rangle}, \quad (8)$$

with ρ being unity at a space point if the spin there did not flip till time t and zero otherwise. The average order parameter for the persistent pattern is

$$\langle \rho(\vec{r}, t) \rangle = \frac{\int d\vec{r} \rho(\vec{r}, t)}{\int d\vec{r}} = P(t). \quad (9)$$

This being a nonconserved (time dependent) quantity and, since, in the definition of $D(r, t)$, the average value is not subtracted from ρ , decorrelation here means, decay of $D(r, t)$ to a ‘‘non-zero’’ value ($=P(t)$), for $t < \infty$. The distance, $\ell_p(t)$, at which $D(r, t)$ reaches this plateau is the characteristic length scale of the pattern. In that case, there may exist scaling of the form

$$\frac{D(r, t)}{P(t)} \equiv f(r/\ell_p). \quad (10)$$

For x ($\equiv r/\ell_p$) > 1 , f should be unity. On the other hand, for fractal dimension d_f and $x < 1$, one should have

$$f(x) \sim x^{d_f - d}, \quad (11)$$

since

$$M \sim x^{d_f}. \quad (12)$$

Considering that $P(t)$, the plateau value, decays in a power-law fashion, a power-law behavior of $f(x)$ is indeed expected, once scaling is achieved. A continuity, at $r = \ell_p$, in such a situation demands

$$t^{(d_f - d)/z} = t^{-\theta}, \quad (13)$$

providing Eq. (5), where z is the dynamic exponent characterizing the growth of the persistence pattern, mentioned before, as

$$\ell_p \sim t^{1/z}. \quad (14)$$

For this model, as mentioned, value of α has been estimated [24] for various T_i values in $d = 2$. However, a priori it is unclear whether there is a general validity of the relation

$$z\alpha = 1. \quad (15)$$

Then it is necessary to calculate both z and θ , for correlated and uncorrelated initial configurations, to validate Eq. (5).

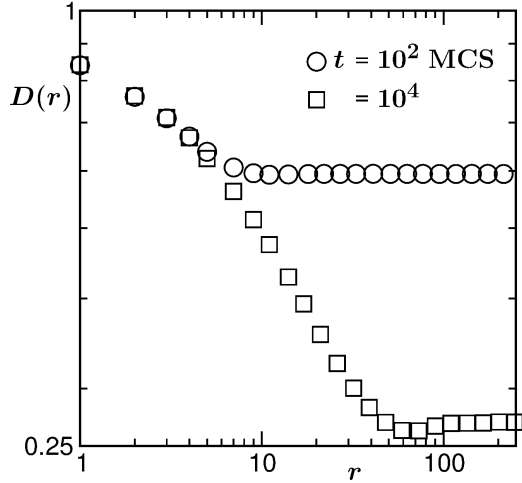


FIG. 4. Density correlation functions, $D(r, t)$, related to the persistent spins, are plotted vs r . Results are presented from two different times, for $T_i = 2.4$ and $T_f = 0$. The system dimensionality is $d = 2$ and value of L is 2048.

IV RESULTS

A. Local Persistence

In Fig. 4 we show $D(r, t)$ as a function of r for $T_i = 2.4$, from two different times, mentioned on the figure, for $d = 2$. As expected, the correlation function decays to different constant value, $P(t)$, at different length ℓ_p , for different times. Before decaying to the plateau, the early time data appear to obey a power-law. The later time data, for smaller r , follows the same power-law before crossing over to another, faster, power-law decay. This implies, there exist two length scales in the problem, below and beyond the equilibrium scale ξ . Inside the larger structure, the small length scale structure remains hidden, which will become irrelevant in the long time limit. For $\xi = \infty$, i.e., $T_i = T_c$, however, the latter will be the only structure and remain for ever. The exponent for large r , for $T_c < T_i < \infty$ and $t \gg 0$, should be related to the d_f value for $T_i = \infty$ case whereas, in case of small r , the exponent should be connected to d_f for $T_i = T_c$ case. Below we focus on these two cases, i.e., $T_i = \infty$ and $T_i = T_c$, separately, first for $d = 2$, followed by $d = 3$.

In the main frame of Fig. 5 we present a scaling exercise [17, 19] for $D(r)$ where we have plotted $f(x)$ as a function of x , using data from different times after quench, for $T_i = T_c$ and $d = 2$. Scaling appears good and gets better with the progress of time. On this log-log plot, look of the data appear, before decaying to unity, linear, implying a power-law decay. The exponent appears to be $\simeq 0.09$. In the inset of this figure, we show analogous exercise for $T_i = \infty$. Even though this case in this dimension was studied by Jain and Flynn [19], for the sake of comparison and

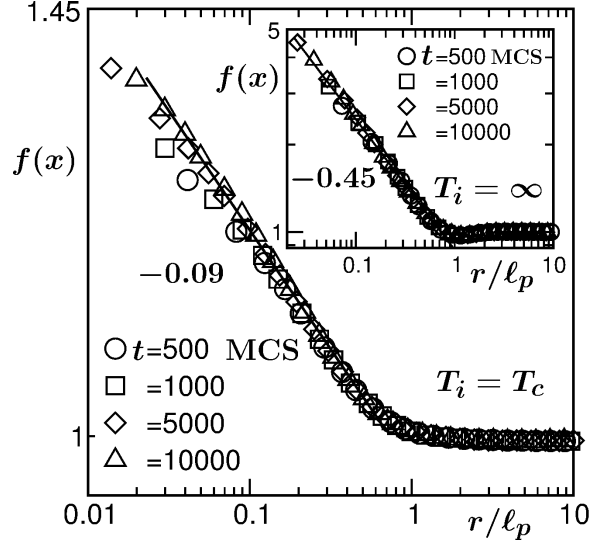


FIG. 5. Scaling analysis of $D(r, t)$ for the $d = 2$ Ising model, with $T_i = T_c$ and $T_f = 0$, where $f(x)$ is plotted vs $x = r/\ell_p$, using data from different times after the quench, on log-log scale. The solid line corresponds to a power-law decay with an exponent 0.09. Inset: Same as the main frame but for $T_i = \infty$. The solid line here has the power-law decay exponent 0.45. The value of L is 2048 for all the results.

completeness, we present it here from our own simulations. In this case, the exponent for the power-law decay appears consistent with 0.45. Then, in $d = 2$, for $T_i = \infty$, the fractal dimensionality is 1.55 and for $T_i = T_c$, the number is 1.91, if Eq. (11) is valid.

In Fig. 6 we show the plots of ℓ_p vs t in $d = 2$, for (a) $T_i = \infty$ and (b) $T_i = T_c$, on log-log scales. In both the cases the data appear consistent with $z = 2$, validating Eq. (15). Nevertheless, we intend to make more accurate quantification. For this purpose, in the insets of these figures we have shown instantaneous exponents, z_i , calculated as [31]

$$\frac{1}{z_i} = \frac{d \ln P}{d \ln t}, \quad (16)$$

vs $1/\ell_p$. For $T_i = \infty$, from this exercise, we quantify $z = 2.2$ and for $T_i = T_c$, we obtain the number $z = 2.1$. These numbers are also consistent with least square fitting of the data to the form

$$\ell_p = \ell_z^0 + A_z t^{1/z}, \quad (17)$$

where ℓ_z^0 and A_z are constants. This may imply, early time corrections to the exponents are insignificant. Note here that, in absence of any correction, one expects [32, 33]

$$\frac{1}{z_i} = \frac{1}{z} \left[1 - \frac{\ell_z^0}{\ell_p} \right], \quad (18)$$

a linear behavior of $1/z_i$, when plotted vs $1/\ell_p$, with slope $-\ell_z^0/z$. However, strong statistical noise in the

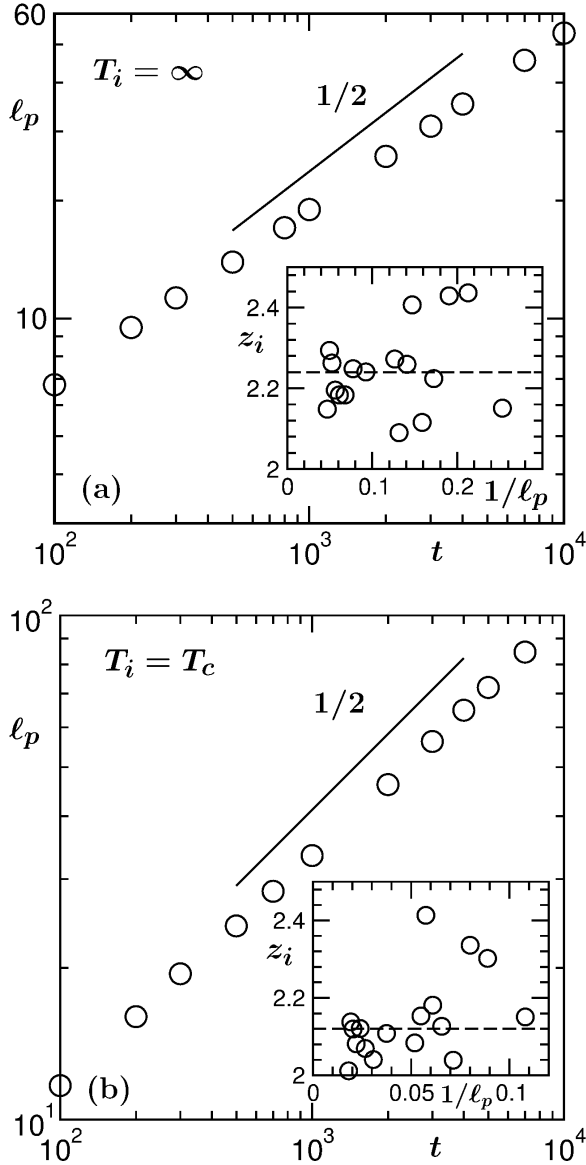


FIG. 6. (a) Log-log plot of persistence length scale, ℓ_p , as a function of t , for $d = 2$ Ising model, following quench from $T_i = \infty$ to $T_f = 0$, with $L = 2048$. Inset: Instantaneous exponent, z_i , obtained using the data in main frame, is plotted vs. $1/\ell_p$. (b) Same as (a), but here $T_i = T_c$. The solid lines in both (a) and (b) correspond to power-law growths with exponent $1/2$. The horizontal dashed lines in the insets correspond to our estimates for z .

data prevents us from doing more accurate analysis and estimation using Eq. (18). Using these values of z , and numbers for θ , mentioned earlier, in Eq. (5), we obtain $d_f = 1.93$ for $T_i = T_c$ and $d_f = 1.51$ for $T_i = \infty$. These values, within computational errors, are consistent with the conclusions from Fig. 5. Next we present results from $d = 3$ where value of α [14, 24] has been previously reported to be $1/3$.

Fig. 7(a) is analogous to the inset of Fig. 5 but for $d = 3$. The exercise for $T_i = T_c$ in $d = 3$ is

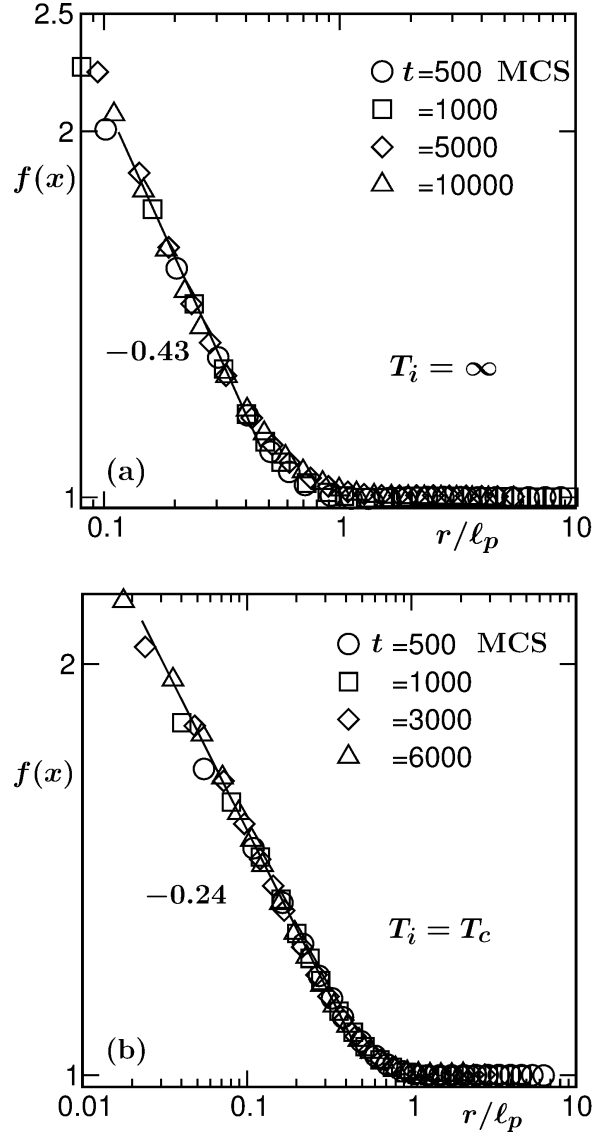


FIG. 7. (a) Scaling function $f(x)$ is plotted vs x , for $d = 3$, $T_i = \infty$ and $T_f = 0$, using data from few different times. The solid line has a power-law decay with exponent 0.43. (b) Same as (a) but, instead of $T_i = \infty$, we present data for $T_i = T_c$. Here the solid line has power-law decay exponent 0.24. The results were obtained for simple cubic lattice with $L = 256$.

presented in Fig. 7(b). Again, for both $T_i = \infty$ and $T_i = T_c$, good data collapse are obtained for results from different times, in these scaling plots. In the relevant region, the $T_i = T_c$ results have power-law decay with exponent 0.24. In case of $T_i = \infty$, the value of this exponent is approximately 0.43. These numbers imply $d_f = 2.76$ and 2.57 for $T_i = T_c$ and $T_i = \infty$, respectively.

In Fig. 8 we show ℓ_p vs t plots from $d = 3$ for (a) $T_i = \infty$ and (b) $T_i = T_c$. In the long time limit, the results for $T_i = \infty$ appear consistent with growth having $z = 3$. Even though this is consistent with Eq.

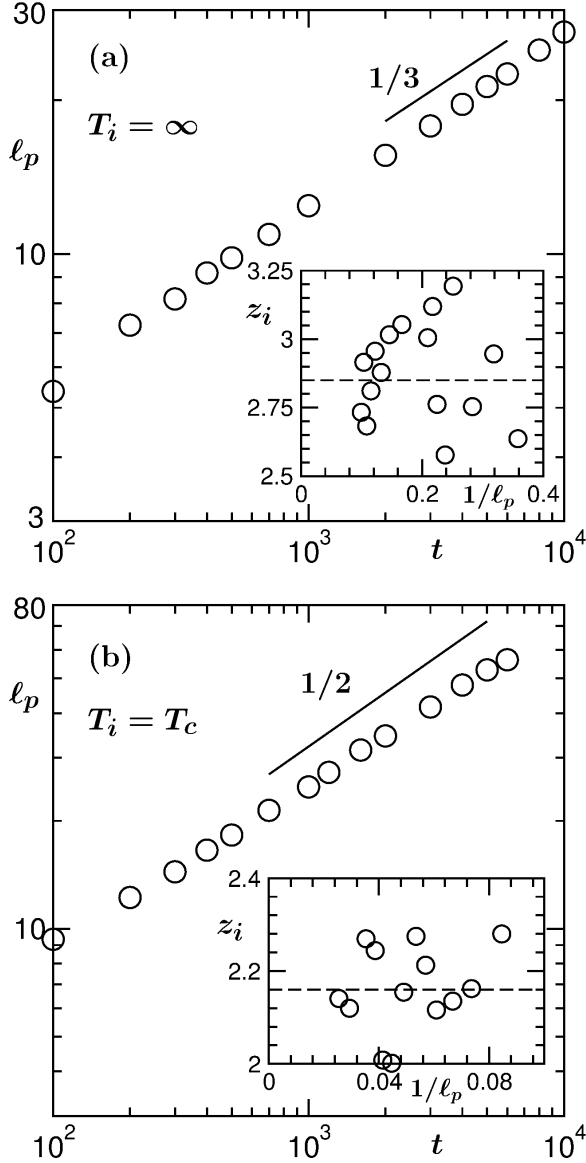


FIG. 8. (a) Log-log plot of ℓ_p vs t from simulations of $d = 3$ Glauber Ising model, for quenches from $T_i = \infty$ to $T_f = 0$. The solid line represents a power-law growth with exponent $1/3$. In the inset we show the corresponding instantaneous exponent, as a function of $1/\ell_p$. (b) Same as (a) but for $T_i = T_c$. The continuous line here represents power-law growth with exponent $1/2$. Again, the inset shows instantaneous exponent z_i , vs $1/\ell_p$. All results correspond to $L = 256$. The horizontal dashed lines in the insets correspond to our estimates for z .

(15), the results for $T_i = T_c$ are in disagreement with this equation if α is still $1/3$, i.e., if α has no dependence upon initial correlation, since, in the latter case, the value of z appears closer to 2. To quantify z more accurately, for both $T_i = \infty$ and $T_i = T_c$, we have shown the instantaneous exponents, vs $1/\ell_p$, in the insets. From there, we extract $z = 2.85$ for $T_i = \infty$ and 2.2 for $T_i = T_c$. This difference is significant and may not be due to numerical error. Thus, it becomes

necessary to directly check the values of α , from the plots of ℓ vs t , which we will do soon. In our earlier work this was done only in $d = 2$. If values of α appear same for both $T_i = \infty$ and $T_i = T_c$, then Eq. (15) becomes invalid. Otherwise, the expectation that α should be independent of initial temperatures, is incorrect. Along with the above mentioned numbers for z , using the values of θ for quenches from $T_i = T_c$ and $T_i = \infty$, we obtain $d_f \simeq 2.77$ and 2.49 . Even though these numbers are consistent with those obtained from the scaling plots in Fig. 7, the discrepancy for $T_i = \infty$ is stronger than in $d = 2$. This can be due to the finite-size effects. Here note that dealing with larger systems in $d = 3$ is significantly difficult. In this context, the results from $d = 2$ corresponds to $L = 2048$ whereas, for $d = 3$, L is 256.

B. Global persistence

Here we look at the global persistence. In the scaling analyses below, involving persistence probabilities calculated using block spins, in addition to estimating new exponents, we will further estimate the values of α in different dimensions and thus check the validity of Eq. (15).

The block persistence was introduced by Cueille and Sire [14], following the Kadanoff blocking concept [5] in renormalization group theory. The corresponding probability P_b , as already mentioned, is related to the change in the order-parameter variable obtained by coarse-graining the site or microscopic spin variables over a block of linear size ℓ_b . It is expected that the decay of this probability will be significantly slower than the site or local persistence probability, to which the former should cross over only for $\ell > \ell_b$. This two time-scale behavior is desirable by considering that, in the early time regime, a slower decay is forced by the fact that a sign change in block spin variable happens only when ℓ becomes comparable to ℓ_b and in the large ℓ limit, the blocks effectively appear as sites. It is expected then that a scaling should be obtained as [14]

$$P_b \ell_b^{\theta_0/\alpha} \equiv h(t/\ell_b^{1/\alpha}), \quad (19)$$

where θ_0 is the exponent of the early part of the decay or global persistence exponent in the sense that when $\ell_b \rightarrow \infty$, this is the only exponent. We aim to check, if best scalings, in accordance with Eq. (17), are obtained for $\alpha = 1/z$ in $d = 2$ and 3 , irrespective of the value of T_i , in addition to the estimation of θ_0 which hitherto were unknown for correlated initial configurations.

In addition to the above mentioned understandings, calculation of persistence probability via such blocking can have advantage for quenches to nonzero temperature. Note that for $T_f \neq 0$, thermal fluctuation

from bulk of the domains affects the calculation when done via standard method. Considering that domain growth occurs essentially due to spin flips along the domain boundaries, in the calculation of P , dynamics inside the domains needs to be discarded. In a method, prescribed by Derrida [12], this is done by simulating an ordered system, alongside the coarsening one, and subtracting the common flipped spins, identifiable as the bulk flips, between the two systems, from the total, thus sticking to the effects of only the boundary motion. In the block spin method, if ℓ_b is significantly larger than ξ at T_f , thermal fluctuations will not alter the sign of block spins and in the large ℓ ($> \ell_b$) limit, as previously stated, one expects the decay to be consistent with local persistence. This saves computational time for simulating the additional systems with ordered configurations.

In Fig. 9(a) we show P_b vs t plots from $d = 2$, for a few different values of ℓ_b and $T_i = T_c$. It appears, as discussed, there exist two step decays and crossover to the faster (consistent with the local persistent decay) one is delayed with increasing ℓ_b .

In Fig. 9(b) we show a scaling exercise using the data of Fig. 9(a) where we have plotted $h(x)$ vs $t/\ell_b^{1/\alpha}$. For obtaining collapse of data, we have adjusted θ_0 and α . The value of α used here is 0.49, that provides the best collapse. This number is certainly consistent with $1/2$, within numerical error. Early time behavior corresponds to global persistence with $\theta_0 = 0.002$ and the late time behavior is consistent with our previous estimation of $\theta_c \simeq 0.035$, for the site persistence probability. In the inset we have shown corresponding scaling results for $T_i = \infty$, for which θ_0 and θ values (mentioned on the figure) are consistent with previous findings [14]. The value of α that provides the best collapse here is 0.5. Note that in our earlier work such independence of α from T_i was directly (from the analysis of ℓ vs t data) checked for this dimension. Following this, similar result was accepted for $d = 3$, without much analysis of the direct results. This we will do in this paper at the end.

In Fig. 10(a) we have presented analogous scaling results from $d = 3$, for $T_i = \infty$. The presented exercise is for best collapse, obtained for $\alpha = 0.37$. Corresponding picture for $T_i = T_c$ is presented in Fig. 10(b) where the value of α is 0.43. In addition, other new results from Fig. 10 are $\theta_0 \simeq 0.058$ for $T_i = \infty$ and $\simeq 0.009$ for $T_i = T_c$. The later time results for both the initial temperatures are consistent with the corresponding site persistence decay exponents.

The values of α , providing best collapse, when multiplied by corresponding values of z , obtained from the analyses in Fig. 8, provide 1 ± 0.06 in this dimension, validating Eq. (15). However, the numbers quoted for both z and α certainly violate the expectation on the independence of these from initial correlations! For

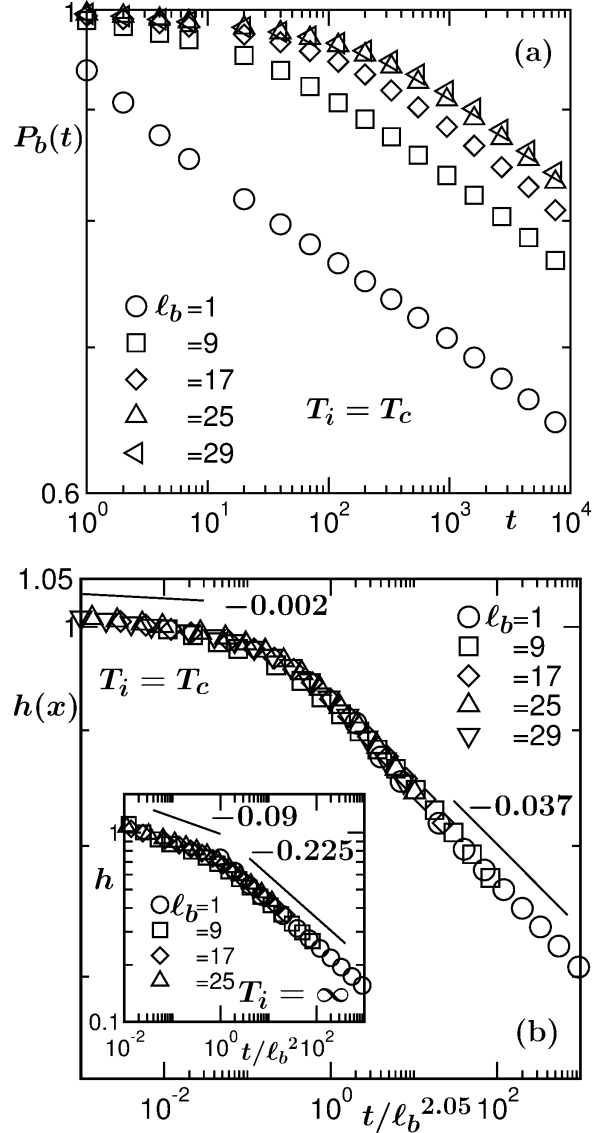


FIG. 9. (a) Plots of block persistence probabilities, vs t , from different values of ℓ_b , for $T_i = T_c$, in $d = 2$. (b) Scaling plots of the persistence probabilities in (a). The scaling function $h(x)$ is plotted, on a log-log scale, vs $x = t/\ell_b^{1/\alpha}$. In the inset of (b) we present similar scaling plot for $T_i = \infty$. System sizes correspond to $L = 2048$. Various power-law decays are shown by solid lines with the exponent values being mentioned next to appropriate lines.

further confirmation, in Fig. 11(a) we present direct plots of ℓ vs t , for both values of T_i in $d = 3$. The data for $T_i = T_c$ are presented in the main frame, whereas the inset contains the results for $T_i = \infty$. The estimation of ℓ was done from the first moment of domain size distribution, $p(\ell_d, t)$, as

$$\ell(t) = \int \ell_d p(\ell_d, t) d\ell_d, \quad (20)$$

where ℓ_d is the distance between two domain boundaries in a particular direction. The solid lines in these

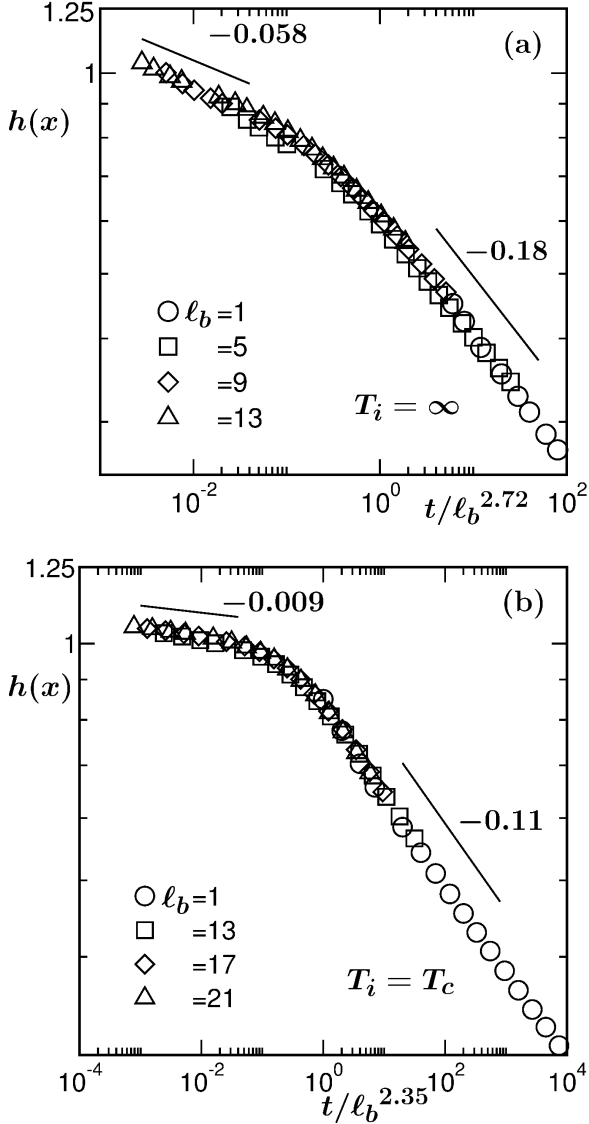


FIG. 10. (a) Same as Fig. 9(b) but for $d = 3$ Ising model and only $T_i = \infty$. (b) Same as (a) but for $T_i = T_c$. Here we have used $L = 256$. Various power-law regimes and corresponding exponent values are pointed out.

plots have power-law behavior with exponents 0.43 and 0.37, the numbers obtained from the scaling exercises in Fig. 10. Both data sets show near consistent behavior with these exponent values. Fitting the data sets to the form (ℓ_α^0 and A_α are constants)

$$\ell = \ell_\alpha^0 + A_\alpha t^\alpha, \quad (21)$$

selecting appropriate regions, we obtain $\alpha = 0.38$ and 0.43 , for $T_i = \infty$ and $T_i = T_c$ respectively. These numbers are in excellent agreement with those obtained from Fig. 10. Further, in Fig. 11(b) we present instantaneous exponents

$$\alpha_i = \frac{d \ln \ell}{d \ln t}, \quad (22)$$

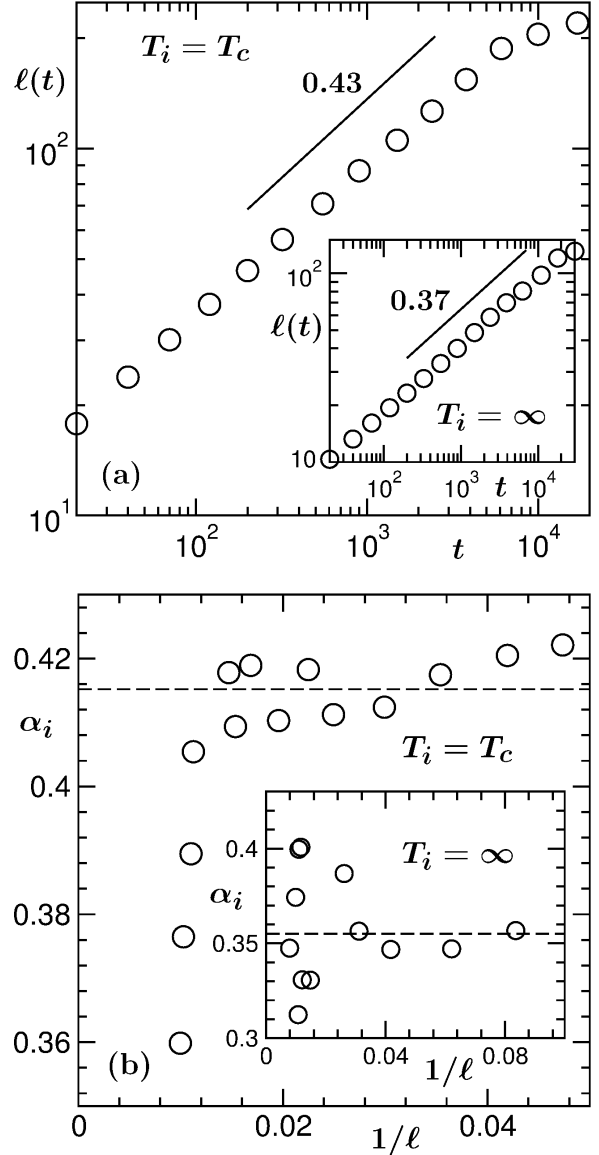


FIG. 11. (a) Plot of average domain length $\ell(t)$ vs. t for quench from $T_i = T_c$ to $T_f = 0$. In the inset we present similar plot for $T_i = \infty$. All results are for $d = 3$ with system size $L = 256$. Solid lines correspond to power-law growths, the exponent values being mentioned next to them. (b) Plots of instantaneous exponents α_i , vs $1/\ell$, from $d = 3$, for $T_i = T_c$ (main frame) and $T_i = \infty$ (inset). The horizontal lines correspond to our estimates for α . For $T_i = T_c$, the sharp fall of the data points, very close to the origin, is due to finite-size effects, which can be appreciated from the direct plot in (a). In the other similar plots, these points were discarded.

for $T_i = T_c$ (main frame) and $T_i = \infty$ (inset). Conclusions from this exercise remain same as above. Then, instead of z , if we use $1/\alpha$, accepting the validity of Eq. (15), in Eq. (5), for $d = 3$ we obtain $d_f = 2.51$ (when $T_i = \infty$) and 2.75 (when $T_i = T_c$). These numbers are in even better agreement with those obtained from Fig. 7.

V CONCLUSION

We have presented results for local and global persistence probabilities for nonconserved Ising model in space dimensions $d = 2$ and 3 , for quenches with initial configurations of varying correlation length ξ . While presented results are mostly related to local persistence [9–13], for the global case [14, 15] we have obtained exponents for quenches from initial temperature $T_i = T_c$, results for which were unknown in both the dimensions. For local persistence, our results are summarized below.

The primary objective of this paper has been to identify the differences in the patterns formed by persistent spins when systems are quenched from $T_i = \infty$ and $T_i = T_c$, to the final temperature $T_f = 0$. For both the cases, corresponding fractal dimensionalities d_f , as well as the exponent z , related to the growth of the persistent pattern, have been obtained in various dimensions. A scaling law connecting d_f , d , z and θ , predicted by Manoj and Ray [17], has been observed to be valid, irrespective of the values of d and T_i . Combining various methods, we quote, for $T_i = \infty$,

$$\begin{aligned} d_f &= 1.53 \pm 0.02, \quad d = 2, \\ d_f &= 2.53 \pm 0.04, \quad d = 3, \end{aligned} \quad (23)$$

and for $T_i = T_c$,

$$\begin{aligned} d_f &= 1.92 \pm 0.02, \quad d = 2, \\ d_f &= 2.75 \pm 0.02, \quad d = 3. \end{aligned} \quad (24)$$

We have also presented direct results for the domain growth in $d = 3$. For both the initial temperatures, the exponent values lie between $1/3$ and $1/2$. The numbers thus obtained are consistent with those providing best collapse in the scaling analyses of block persistence probabilities, as well as with the ones obtained from the analyses of characteristic lengths for the persistence pattern. Unlike in $d = 2$, these findings indicate that there exist initial correlation dependence in the domain growth in $d = 3$. Here it is worth mentioning that theoretically the value of α is expected to be $1/2$, irrespective of the system dimension. Except for $T_i = \infty$ in $d = 3$, in all other cases the results are nearly consistent with the expectation. An understanding should then be obtained for the discrepancy for $T_i = \infty$ in $d = 3$. On the other hand, the direct domain patterns for $T_i = T_c$ is non-self-similar in nature. Thus, to understand the difference that exists between the two cases, i.e., for $T_i = \infty$ and $T_i = T_c$, one needs further studies. However, since, scaling analyses of other quantities provide quantitatively similar numbers for the two cases, the difference may be real. On the other hand, from the renormalization group theoretical consideration, one expects

no such difference. All these comments lead to the necessity of revisiting the $d = 3$ case for $T_i = \infty$.

In future we will address similar issues for conserved order parameter dynamics, including aging phenomena. For both conserved and nonconserved dynamics, scaling properties and form of the two-point correlation function will be an important problem for the case of correlated initial configurations.

ACKNOWLEDGEMENT

The authors thank Department of Science and Technology, Government of India, for financial support. SKD acknowledges hospitality and financial supports from International Centre for Theoretical Physics, Italy. He is also thankful to the Marie Curie Actions Plan of European Commission (FP7-PEOPLE-2013-IRSES grant No. 612707, DIONICOS).

* das@jncasr.ac.in

-
- [1] A. Onuki, *Phase Transition Dynamics*, Cambridge University Press, Cambridge, UK (2002).
 - [2] A. J. Bray, *Adv. Phys.* **51**, 481 (2002).
 - [3] R. A. L. Jones, *Soft condensed matter*, Oxford University Press, Oxford, Oxford (2008).
 - [4] A. J. Bray, S. N. Majumdar and G. Schehr, *Adv. Phys.* **62**, 225 (2013).
 - [5] N. Goldenfeld, *Lecture Notes on Phase Transitions and the Renormalization Group*, Addison-Wesley, Reading, MA (1992).
 - [6] D. S. Fisher and D. A. Huse, *Phys. Rev. B* **38**, 373 (1988).
 - [7] F. Corberi, E. Lippiello and M. Zannetti, *Phys. Rev. E* **74**, 041106 (2006).
 - [8] J. Midya, S. Majumder and S. K. das, *J. Phys. : Condens. Matter* **26**, 452202 (2014).
 - [9] S. N. Majumdar, C. Sire, A. J. Bray and S. J. Cornell, *Phys. Rev. Lett.* **77**, 2867 (1996).
 - [10] S. N. Majumdar, A. J. Bray, S. J. Cornell and C. Sire, *Phys. Rev. Lett.* **77**, 3704 (1996).
 - [11] B. Derrida, V. Hakim and R. Zeitak, *Phys. Rev. Lett.* **77**, 2871 (1996).
 - [12] B. Derrida, *Phys. Rev. E* **55**, 3705 (1997).
 - [13] D. Stauffer, *Int. J. Mod. Phys. C* **8**, 361 (1997).
 - [14] S. Cueille and C. Sire, *J. Phys. A: Math and Gen.* **30**, L791 (1997).
 - [15] S. Cueille and C. sire, *European Phys. J. B* **7**, 111 (1999).
 - [16] G. Manoj and P. ray, *Phys. Rev. E* **62**, 7755 (2000).
 - [17] G. Manoj and P. ray, *J. Phys. A: Math and General* **33**, 5489 (2000).
 - [18] G. Manoj and P. ray, *J. Phys. A: Math and General* **33**, L109 (2000).
 - [19] S. Jain and H. Flynn, *J. Phys. A: Math and General* **33**, 8383 (2000).
 - [20] M. Saharay and P. Sen, *Physica A* **318**, 243 (2003).

- [21] D. Chakraborty and J. K. Bhattacharjee, Phys. Rev. E **76**, 031117 (2007).
- [22] R. Paul, A. Gambassi and G. Schehr, Europhys. Lett. **78**, 10007 (2007).
- [23] T. Blanchard, L. F. Cugliandolo and M. Picco, J. Stat. Mech. P12021 (2014).
- [24] S. Chakraborty and S. K. Das, European Phys. J. B **88**, 160 (2015).
- [25] C. Dasgupta and R. Pandit, Phys. Rev. B **33**, 4752 (1986).
- [26] K. Humayun and A. J. Bray, J. Phys. A: Math and Gen. **24**, 1915 (1991).
- [27] A. Sicilia, J. A. Arenzon, A. J. Bray and L. F. Cugliandolo, Phys. Rev. E **76**, 061116 (2007).
- [28] D. P. Landau and K. Binder, *A Guide to Monte Carlo Simulations in Statistical Physics*, Cambridge University Press, Cambridge (2009).
- [29] R. J. Glauber, J. Math. Phys. **4**, 294 (1963).
- [30] U. Wolff, Phys. Rev. Lett. **62**, 361 (1989).
- [31] D. A. Huse, Phys. Rev. B **34**, 7845 (1986).
- [32] J. G. Amar, F. E. Sullivan and R. D. Mountain, Phys. Rev. B **37**, 196 (1988).
- [33] S. Majumder and S. K. Das, Phys. Rev. E **81**, 050102 (2010).